

Supplemental Information

Characterization of the Immune Cell

Infiltration Landscape in Head and Neck

Squamous Cell Carcinoma to Aid Immunotherapy

Xinhai Zhang, Mengqi Shi, Tielou Chen, and Boxin Zhang

**Characterization of the immune cell infiltration landscape in head and neck
squamous cell carcinoma to aid immunotherapy**

Xinhai Zhang², Tielou Chen² and Boxin Zhang¹

¹ Department of Stomatology, Changzheng hospital, Second military Medical University, Shanghai 200003, China

² Oral Research Center of CPLA, Changhai hospital, Second military Medical University, 15 Dongjiangwan Road, Shanghai 200081, China

Correspondence should be addressed to Boxin. Zhang (s441566391@163.com)

* Corresponding author: Boxin. Zhang, Department of Stomatology, Changzheng hospital, Second military Medical University, Shanghai 200003, China

E-mail: s441566391@163.com

TEL: 86-21-56715915

Figure S1. Overview of study design and consensus matrixes of all HNSC samples

A Exploratory analysis

Fraction of 1029 HNSC cancers' Tumor-infiltrating immune cells from gene-expression profiling datasets.
(TCGA, GSE41613, GSE42743, GSE65858, and E-MTAB-1328)

Consensus clustering algorithm for immune cells infiltrating patterns
ICI cluster A
ICI cluster B
ICI cluster C

Identify genes associated with ICI

Discovery study

Consensus clustering algorithm of DEGs to classify patients in TCGA cohort into three groups
Gene cluster A
Gene cluster B
Gene cluster C

ICI signature genes A

ICI signature genes B

Brouta algorithm

PCA algorithm

ICI score A

ICI score B

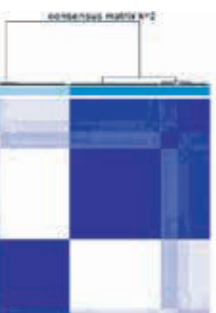
ICI score = ICI score A - ICI score B

Validation study

Validate the prognostic value of ICI score in GSE41613, GSE65858, GSE42743, and all HNSC cohort.

Evaluating the predictive value of ICI score for immunotherapy in IMvigor210 and TCGA-SKCM cohorts.

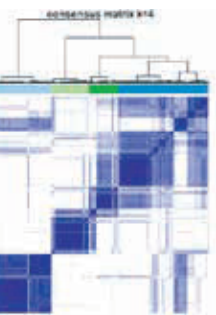
B



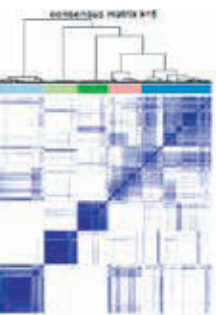
C



D

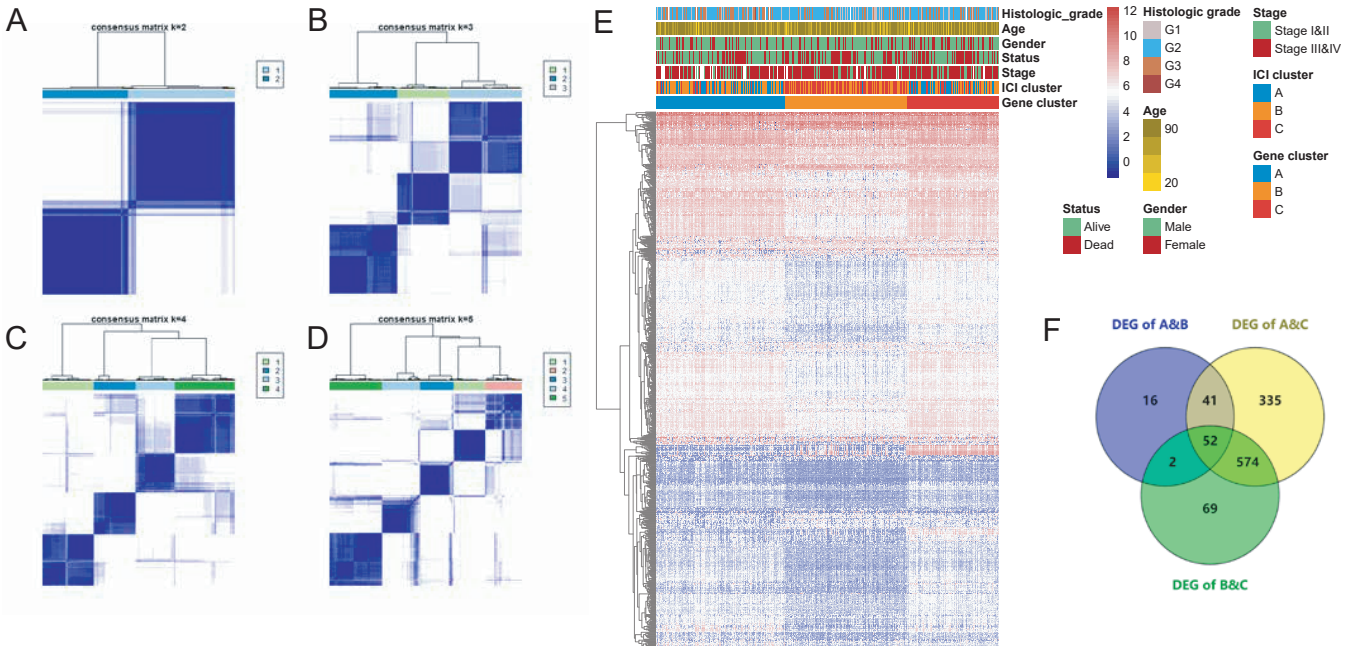


E



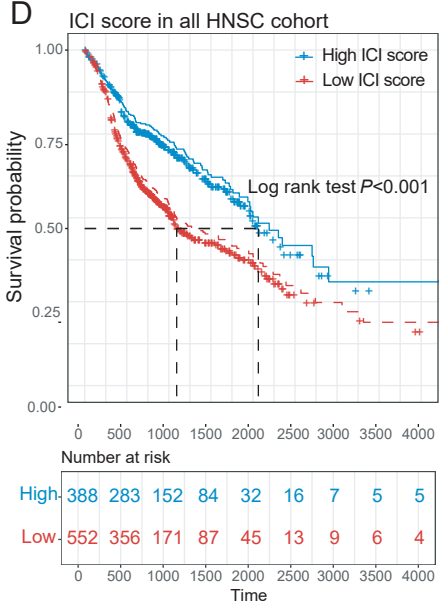
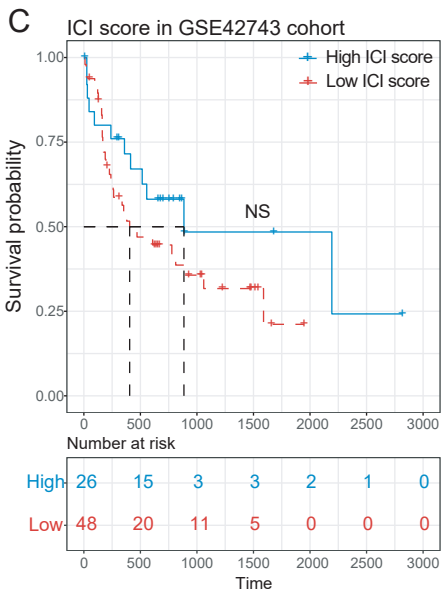
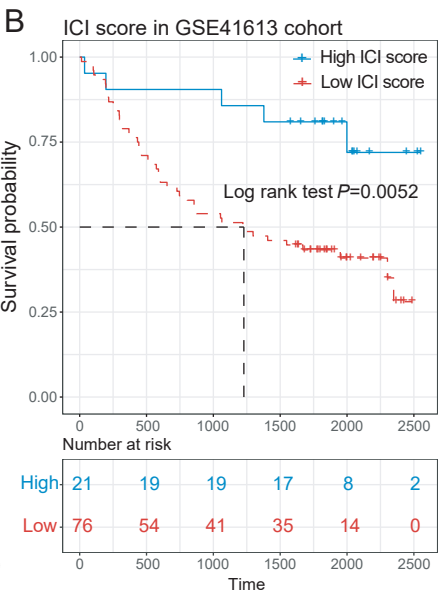
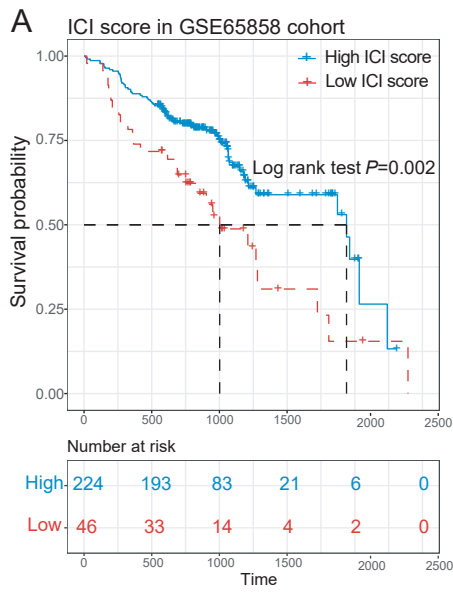
A. Overview of study design. **B.** Consensus matrixes of all HNSC samples for each k ($k = 2-5$), displaying the clustering stability using 1000 iterations of hierarchical clustering.

Figure S2. Consensus clustering of TME cell infiltration in the ACRG cohort and DEGs among the ICI phenotypes



A-D. Consensus matrixes of TCGA-HNSC cohorts for each k ($k = 2-5$), displaying the clustering stability using 1000 iterations of hierarchical clustering. **E.** Unsupervised clustering of 1089 DEGs among three ICI cluster groups to classify patients in TCGA-HNSC into three groups. **F.** Venn diagram illustrating the number of DEGs among the three ICI clusters.

Figure S3. Prognostic value of ICI scores in HNSC cohorts.



A. Kaplan–Meier curves for patients with high and low ICI scores in the GSE65858 cohort. Log-rank test $P=0.002$. **B.** Kaplan–Meier curves for patients with high and low ICI scores in the GSE41613 cohort. Log-rank test $P=0.0052$. **C.** Kaplan–Meier curves for patients with high and low ICI scores in the GSE42743 cohort. **D.** Kaplan–Meier curves for patients with high and low ICI scores in the all HNSC cohort. Log-rank test $P<0.0001$.